2-14-2019

Vertical Marine Snow Distribution in the Stratified Hypersaline, and Anoxic Orca Basin (Gulf of Mexico)

Arne Diercks
University of Southern Mississippi, Arne.Diercks@usm.edu

Kai Ziervogel
University of New Hampshire

Ryan Sibert
University of Georgia

Samantha B. Joye
University of Georgia

Vernon Asper
University of Southern Mississippi

ELEMENTA
Science of the Anthropocene

Diercks, A, et al. 2019. Vertical marine snow distribution in the stratified, hypersaline, and anoxic Orca Basin (Gulf of Mexico). *Elem Sci Anth,* 7: 10. DOI: https://doi.org/10.1525/elementa.348

RESEARCH ARTICLE

Vertical marine snow distribution in the stratified, hypersaline, and anoxic Orca Basin (Gulf of Mexico)

Arne Diercks*, Kai Ziervogel†, Ryan Sibert‡, Samantha B. Joye‡, Vernon Asper* and Joseph P. Montoya§

We present a complete description of the depth distribution of marine snow in Orca Basin (Gulf of Mexico), from sea surface through the pycnocline to within 10 m of the seafloor. Orca Basin is an intriguing location for studying marine snow because of its unique geological and hydrographic setting: the deepest ~200 m of the basin are filled with anoxic hypersaline brine. A typical deep ocean profile of marine snow distribution was observed from the sea surface to the pycnocline, namely a surface maximum in total particle number and midwater minimum. However, instead of a nepheloid (particle-rich) layer positioned near the seabed, the nepheloid layer in the Orca Basin was positioned atop the brine. Within the brine, the total particle volume increased by a factor of 2–3 while the total particle number decreased, indicating accumulation and aggregation of material in the brine. From these observations we infer increased residence time and retention of material within the brine, which agrees well with laboratory results showing a 2.2–3.5-fold reduction in settling speed of laboratory-generated marine snow below the seawater-brine interface. Similarly, dissolved organic carbon concentration in the brine correlated positively with measured colored dissolved organic matter (r^2 = 0.92, n = 15), with both variables following total particle volume inversely through the pycnocline. These data indicate the release of dissolved organic carbon concomitant with loss in total particle volume and increase in particle numbers at the brine-seawater interface, highlighting the importance of the Orca Basin as a carbon sink.

Keywords: Gulf of Mexico; Orca Basin; Marine Snow; CDOM; DOC; Brine Lake

Introduction

Orca Basin is a morphologically isolated, intraslope depression on the Louisiana continental slope of the northern Gulf of Mexico. Since its first description by Shokes et al. (1977), the Basin has been the focus of interdisciplinary studies due to its unique geological and morphological characteristics and its strong stratification and permanent halocline (Murray, 1966; Shokes et al., 1977; McKee et al., 1978; Wiesenburg, 1980; Sheu, 1983; Wiesenburg et al., 1985; Sheu and Presley, 1986a, 1986b; Van Cappellen et al., 1998; Tribovillard et al., 2009). The stratified geochemistry of Orca Basin is somewhat unique as a small enclosed basin situated in a larger body of normal seawater (Shokes et al., 1977), but it is also comparable to that of other anoxic, deep-sea brines in the Black Sea (Kaminskii et al., 1989; Wei and Murray, 1994; Hurtgen et al., 1999) and Red Sea (Schardt, 2016).

* The University of Southern Mississippi, Stennis Space Center, MS, US
† University of New Hampshire, Durham, NH, US
‡ The University of Georgia, Athens, GA, US
§ Georgia Institute of Technology, Atlanta, GA, US
Corresponding author: Arne Diercks (arne.diercks@usm.edu)

The deep bottom waters of Orca Basin have been hypersaline for at least the last 7,900 years (Addy and Behrens, 1980; Leventer et al., 1983; Meckler et al., 2008; Shah et al., 2013). Sediments of the basin were reported as anoxic, dark in color, and strongly reducing, transitioning to grey mud below 4.85 m (Addy and Behrens, 1980). Data from gravity cores indicated that porewater salinity in these sediments decreased from 238 near the sediment-water interface to 112 at 10.79 m depth, suggesting brine entrainment from surrounding slopes rather than upward diffusion from underlying sediments (Addy and Behrens, 1980). Sheu et al. (1988) and Pilcher and Blumstein (2007) attributed the formation of the Orca brine to the dissolution of shallow subsurface salt diapirs exposed to seawater by seafloor slumping, present in at least three distinct locations within the basin. This accumulation of brine has generated a strong halocline in Orca Basin, with salinity abruptly increasing from 35 to >275 between water depths of 2,230 m and 2,260 m. This pycnocline temporarily traps settling material within the transition zone between seawater and brine.

Sinking particles rich in organic matter (i.e., marine snow) are major drivers of the biological pump that removes organic carbon from the surface ocean, sequestering atmospheric CO_2 in the deep ocean (Ducklow et al.,

2001). The settling speed of marine snow in the ocean is influenced by water column stratification (Prairie et al., 2013, 2015), as particle velocity depends on the excess density of the particle relative to that of the surrounding water mass. When particles reach a zone of increased density, settling speed decreases proportionally to the loss in excess density (Condie and Bormans, 1997; Kindler et al., 2010; Prairie et al., 2013, 2015; Prairie and White, 2017). The integrity of a particle then depends on the amount of time that it remains suspended at this depth. Residence time within the transition zone strongly influences remineralization, breakage, reaggregation and partial dissolution of marine snow particles, as they are exposed to numerous physical, chemical, and biological alterations that can reshape parts or all of the individual particles. The deep Orca Basin pycnocline serves as a particle trap: Van Cappellen et al. (1998) observed that the highest concentration of particulate Mn in Orca Basin occurred at 2,200 m, in the middle of the chemocline/pycnocline that reflects a broad seawater-to-brine transition zone.

Limited information is available about the distribution of marine snow within Orca Basin, most of which is based on unpublished video data from manned submersible dives (S Joye, pers. observation). Here, we provide the first profile of marine snow concentration from the sea surface to within 10 m of the seafloor in the northern Orca Basin obtained using an in situ marine snow camera. We highlight a detailed set of our data that focus on the water column across the pycnocline from 2,150 m to 2,275 m. Below this depth, salinity is generally uniform. This section of the water column is characterized by a rapid increase in particle concentration and salinity, a decrease in temperature and oxygen availability, and the associated physical and chemical transformations of organic and inorganic materials.

Methods

Bathymetry

Individual isobaths corresponding to the top of the transition zone from seawater to brine (2,140 m) and the top of the brine (2,251 m) were computed from the high resolution bathymetry data of Kramer and Shedd (2017) within the enclosed area of the Orca Basin (**Figures 1** and S1) using Blue Marble Geographics GIS software package Global Mapper© (Software Version 16.2.7). The volumes within each isobath were calculated using the 'volume' function of the software package. The sum of these volumes was used to determine the total volume of the brine and transition zone.

Profiling camera

A profiling camera system similar to the one published by Honjo et al. (1984) and Asper (1987) was used during Endeavor cruise EN586 in August 2016 to document the vertical distribution of marine particles larger than 0.2 mm in diameter along depth within the northern Orca Basin

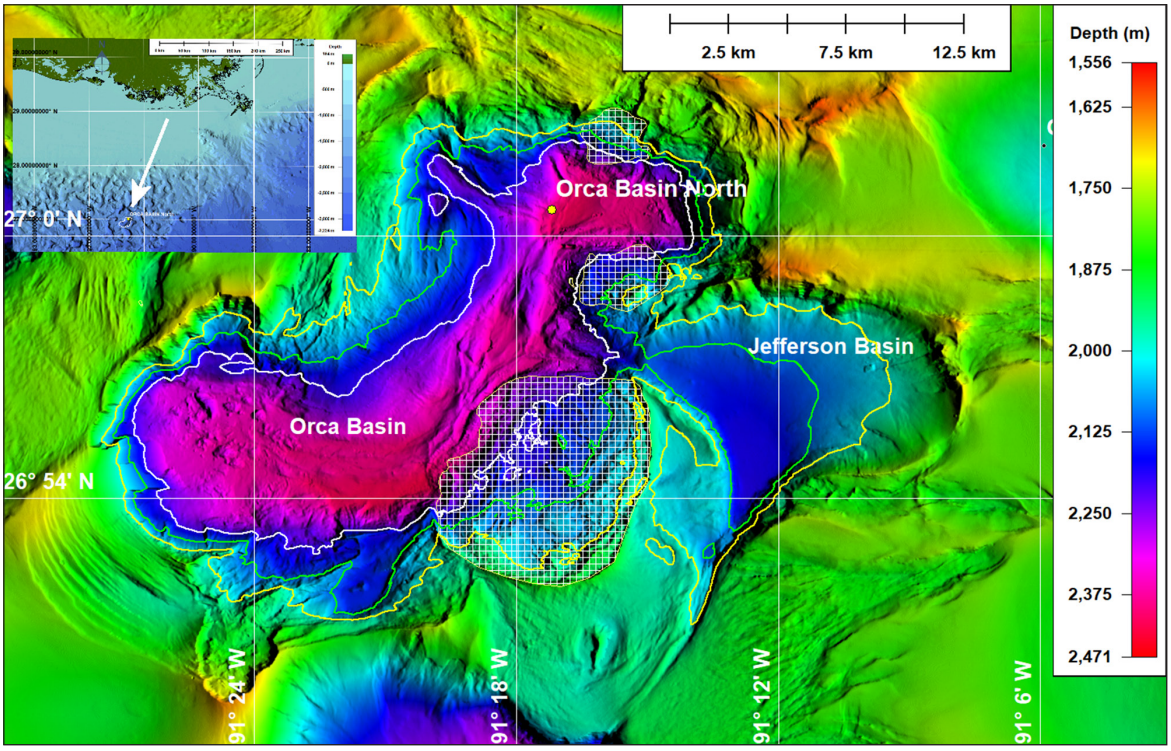

Figure 1: Overiew map of Orca Basin, northern Gulf of Mexico. Insert in upper left corner depicts location of enlargement on Louisiana continental slope. Yellow line depicts 2,000 m isocline; green and white lines present the 2,100 m and 2,200 m isoclines, respectively. The yellow dot labeled Orca Basin North marks the position of the camera cast. The white hatched areas present the extent of salt exposure mapped atop the recently published high resolution seafloor morphology by the Bureau of Ocean and Energy Management (BOEM; https://www.data.boem.gov/Main/Mapping.aspx; Kramer and Shedd, 2017). DOI: https://doi.org/10.1525/elementa.348.f1

(27° 00.287′ N; 91° 17.560′ W) (**Figure 1**). The standard configuration of the marine snow profiling camera system included a Nikon 7000 digital single-lens reflex camera, a SeaBird Seacat-19 CTD, and a light transmissometer. For the deployment in this study, a WET Labs Environmental Characterization Optics Fluorometer and Scattering Meter (ECO-FLNTU) for turbitity measurements and a WET Labs ECO Fluorometer (ECO-FL) to measure colored dissolved organic matter (CDOM; 460 nm) were also included. Lead weights (136 kg) were added to the camera frame to compensate for the anticipated density increase within the brine. Camera metadata of frame number, time, and exposure settings were recorded with each image and matched to the corresponding CTD time to determine the depth of each image.

Two strobe heads illuminated a section of the undisturbed water column through two collimators mounted perpendicularly 60 cm in front of the camera. Image blackouts, as observed during the camera profile presented here, can occur when the light emitted by the two strobe units is not received by the imaging chip inside the Nikon D7000 camera. The internal factory intervalometer of the Nikon D7000 camera allowed a total of 999 images to be captured per deployment. A high-powered 12 kHz pinger (Oceanographic Instrument Systems, Inc.) was mounted to the camera frame to track the package during its descent through the water column, determine its depth, and gauge the distance to the seafloor using the shipboard echo sounder. Imaging terminated about 10 m above the seafloor.

The camera lowering speed was timed to achieve a high vertical resolution of particle distribution within the halocline near 2,200 m water depth. At an intervalometer setting of 7 seconds between images, the initial lowering speed was set to 25 m min^{-1} capturing images at a vertical separation of 2.9 m. Below 2,080 m the camera was lowered at 15 m min^{-1} to a depth of 2,234 m increasing the vertical depth resolution to 1.75 m per image. Winch descent speed was increased to 25 m min^{-1} between 2,234 m and 2,406 m (max depth) and for recovery. A total of 973 images were recorded, generating an uninterrupted profile that spanned the water column from the surface to a pressure depth of 2,406 m. Image depths were determined by correlating the times recorded from the synchronized CTD data with the time stamps recorded within the exchangeable image file data stored with each image.

All images were processed using Image-Pro® software. The camera was calibrated by placing a reference object of known size within the camera's focal point. Based on the illuminated area in the images, an area of interest was selected, the dimensions measured, and a volume of illuminated water calculated. All particles larger than 0.2 mm in diameter were counted and sized. Any identifiable objects that were not marine snow (e.g., bubbles, zooplankton, fish, etc.) were marked and removed before the counting of particles per image. Counted particles were normalized to volume and binned by size. During post-processing, particles were binned in 10-m vertically averaged bins.

Settling chamber experiments

Laboratory sinking experiments were conducted to estimate the settling behavior of particles across the strong density gradient observed in the Orca Basin. Marine snow particles were formed in roller tanks filled with a senescent diatom culture and coastal seawater at equal volumes (total tank volume: 1.25 L) and incubated on a roller table at 3.5 rpm at room temperature for ~20 h. The settling experiment was performed at room temperature using filtered seawater and Orca Basin brine in a graduated cylinder. Eleven individual aggregates were siphoned into separate Petri dishes containing Gulf of Mexico bottom water (collected at a water depth of 1,600 m) and the aggregates were soaked for ~2 h. Aggregates were then photographed with a digital microscope (Model 26700-300, Aven Inc.), producing images of the two-dimensional projection of the aggregate. Aggregate settling behaviors were studied in a 1.5-L graduated glass cylinder containg seawater on top of Orca Basin brine. The cylinder was filled as described in Prairie et al. (2017) by slowly pouring the seawater through a diffuser onto the top of the brine. The brine layer at the base of the cylinder was 18 cm thick, the transition zone 2.5 cm, and the overlying seawater 16 cm. For each individual aggregate, we recorded the settling speed and time spent in the distinct layers.

Geochemical analyses

Two CTD profiles were obtained by the Endeavor's Sea-Bird SBE 9 rosette CTD near the camera site in the northern Orca Basin. Water samples for laboratory measurement of concentrations of dissolved organic carbon (DOC), chloride, sodium, potassium, magnesium, and calcium were collected during CTD cast EN_005.03 in the northern Orca Basin. DOC samples were filtered (0.2 μm) and stored frozen until analysis. Samples for determining major ion concentrations were filtered (0.2 μm), acidified with concentrated nitric acid to a pH < 1, mixed well, sealed tightly and stored at room temperature until analysis. Concentrations of DOC were determined using a Shimadzu TOC-V equipped with a nondispersive infrared detector and employing a high temperature catalytic oxidation method; reagent grade potassium hydrogen phthalate was used as the DOC standard. Concentrations of chloride, sodium, potassium, magnesium, and calcium were determined using a Dionex ion chromatrography system; separate runs were employed to quantify anions and cations. Ion chromatography standards were generated using National Institute of Standards and Technology-certified ion standards. For this paper the measured CTD salinity data were used up to a salinity of 90. Salinities in the brine with higher concentrations were estimated using Knudsen's modified relationship: salinity = 1.80655 * chloride (Joint Panel on Oceanographic Tables, 1966).

Results

Basin morphology

The size of Orca Basin was recalculated based on the high resolution bathymetry by Kramer and Shedd (2017). We propose that the previously suggested 1,800 m depth

contour as the border for the Orca Basin be lowered to 2,100 m, as the 1,800-m isobath extends downslope beyond the actual confines of the Basin into other morphologically independent areas (**Figures 1** and S1). This change in depth limit for the Basin reduces the 2-D surface area from ~400 km^2 (Shokes et al., 1977) to ~224 km^2. A permanent halocline is present near the 2,200-m isobath, approximately 200 m above the seafloor (Sheu, 1990; Tribovillard et al., 2008), covering an area of ~150 km^2. For the purpose of this discussion, we define the limits of the transition zone between seawater and brine to cover depths from 2,140 m to 2,251 m. This 111-m thick transition zone has a calculated volume of 16.76 km^3 (enclosed area of 258 km^2, measured at the upper depth limit), and the brine volume is 10.24 km^3 (enclosed area of 158 km^2). Pilcher and Blumstein (2007) suggest the source of the salt was the top of a salt dome that was exposed due to over-steepening slopes and subsequent slumping of the sediment covering the salt. Water outflow from the deep Basin is limited by a morphological sill located in the NE of the Basin, allowing water to drain into Jefferson Basin at 2,232 m depth (**Figure 1**). An additional sill at 2,100 m depth is located about 1 km to the East of the 2,200-m isobath restricting the outflow even further (**Figure 1**; Kramer and Shedd, 2017).

Camera data

The total particle volume in each image, analyzed and calculated based on the mean particle diameter measured during the image processing, did not vary much from the surface to a depth of 2,225 m. At 2,225 m a single peak was observed, located above the maximum in beam attenuation. At this depth, the total volume of aggregates increased by two orders of magnitude from an average (±standard deviation) of 6.1 ± 0.3 mm^3 (0 to 2,229 m, n = 803) to 600 ± 0.3 mm^3 (2,229 m, n = 1) measured within a single image. The total particle volume within the brine, between 2,229 m and 2,402 m, averaged 21.0 ± 2.2 mm^3 (n = 57).

Particle data (**Table 1**) grouped into two size classes, <1.0 mm and >1.0 mm equivalent spherical diameter (ESD), and beam attenuation data revealed a strong nepheloid layer just above the brine, with another layer at a depth of 2,198 m in terms of total particle number but not total particle volume (**Figures 2**, **3**, and S2). The first signs of increased particle concentrations were recorded below 1,600 m, where concentration steadily increased to 63.5 particles L^{-1} at 2,000 m (**Figures 2** and **3**). Below the pycnocline the smaller size fraction diminished in concentration and the abundance of larger particles doubled from 2.1 L^{-1} above the pycnocline to 4.5 L^{-1} in the brine. Total particle volume doubled below the pycnocline from 0.7 mm^3 L^{-1} to 1.4 mm^3 L^{-1}. Large particles made up 10.7% of the enumerated particles in the upper 200 m of the water column; below 200 m to a depth of 1,600 m, the concentration of both size fractions varied little, with large particles present at 2.2–5.3% of the total particle concentration (**Table 1**). Below 1,600 m to a depth of 2,251 m, particle concentration in both size classes increased; however, the larger particles only comprised 2.2–3.2% of the total particle load. In the brine, below 2,251 m, the concentration of large particles doubled and the larger particle size fraction increased by a factor of three (**Table 1**).

Water column data from both the camera-mounted CTD and the ship's CTD indicated the same vertical structure of surface mixed layer, midwater column minima in salinity

Table 1: Characteristics of the vertical distribution of marine snow in Orca Basin. DOI: https://doi.org/10.1525/elementa.348.t1

Depth (m)		Total particle number (L^{-1})[a]				% of total number > 1.0 mm	Total particle volume (L^{-1})[b]		n
From	To	<1.0 mm	Std. Dev.	>1.0 mm	Std. Dev.		mm^3	Std. Dev.	
0	200	11.3	1.6	1.3	0.3	10.7	0.9	0.13	71
200	400	14.4	2.2	0.6	0.1	3.9	0.6	0.12	73
400	600	12.5	1.9	0.6	0.1	4.4	0.6	0.68	71
600	800	13.2	1.9	0.6	0.1	4.4	0.5	0.07	67
800	1,000	10.3	1.4	0.6	0.1	5.3	0.5	0.07	65
1,000	1,200	10.0	1.4	0.5	0.1	4.5	0.4	0.06	66
1,200	1,400	11.4	1.7	0.5	0.1	4.1	0.5	0.11	67
1,400	1,600	14.4	2.2	0.6	0.1	3.9	0.5	0.08	66
1,600	1,800	21.4	3.6	0.6	0.2	2.8	0.5	0.15	68
1,800	2,000	35.7	6.3	0.8	0.2	2.2	0.6	0.13	67
2,000	2,200	63.5	10.7	2.1	0.7	3.2	0.9	0.13	105
2,200	2,400	48.0	8.9	4.5	1.2	8.6	2.6	2.27	71

[a] Particle distribution in the water column, averaged for 200-m depth bins and grouped by size: <1.0 mm equivalent spherical diameter (ESD) and >1.0 mm ESD.

[b] Total particle volume was calculated based on ESD.

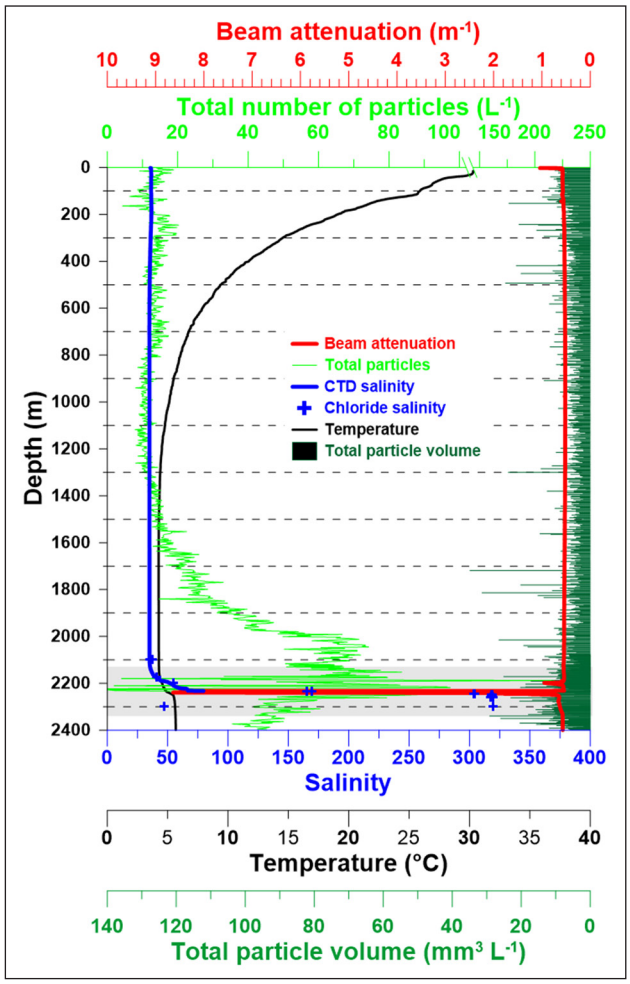

Figure 2: Water column profile of camera data. Data obtained by the camera profile in the northern Orca Basin area are presented. Blue line represents salinity, red line beam transmission, black line temperature and green line the number of particles encountered during the camera cast. Total particle volume is shown as black horizontal bars. Grey box between 2,140 m and 2,340 m presents the area of the detailed enlargement in Figure 3. CTD salinity was plotted to a value of 90; blue crosses indicate salinity as calculated from chloride ion concentration using the relationship of salinity = 1.80655 * chloride (Table 1). DOI: https://doi.org/10.1525/elementa.348.f2

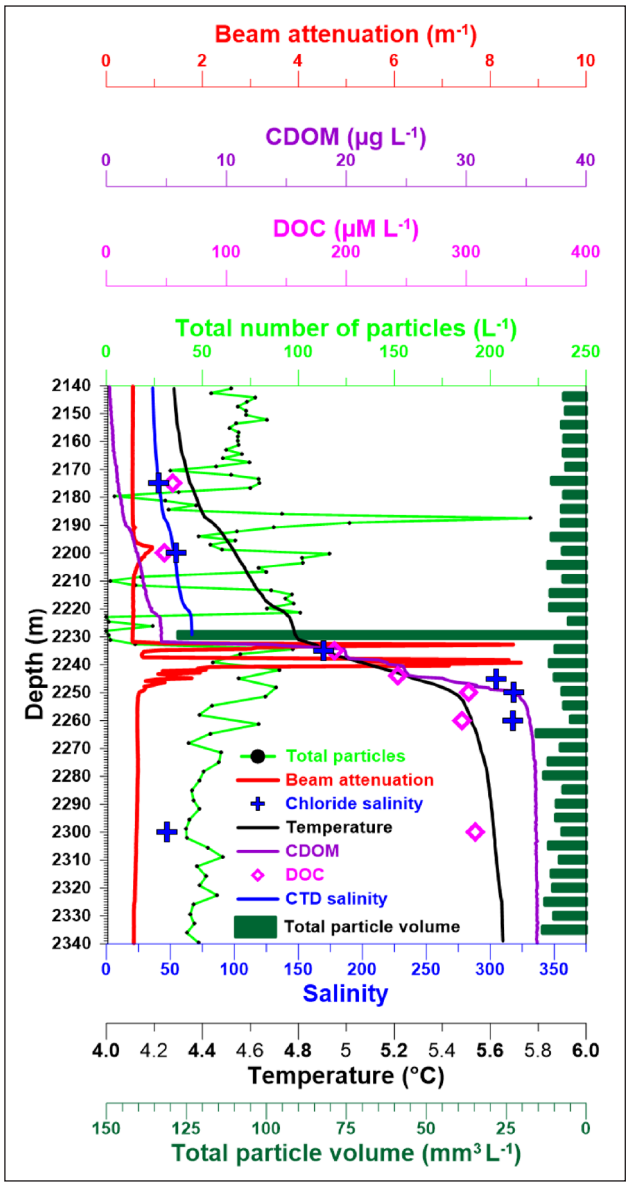

Figure 3: Enlargement of transition zone between seawater and brine. Total particle numbers are presented as green line with black dots. Total particle volume is shown as black horizontal bars. DOC and CDOM are presented as purple diamonds and line, respectively. Temperature, salinity and beam transmission are indicated by lines in black, blue and red, respectively. CTD salinity was plotted to a value of 90; blue crosses indicate salinity as calculated from chloride ion concentration using the relationship of salinity = 1.80655 * chloride (Table 1). DOI: https://doi.org/10.1525/elementa.348.f3

and temperature and steep increase in salinity concentration at the depth of the pycnocline (see Figure S3 for a temperature–salinity plot). The oxygen profile taken by the ship's CTD showed a rapid decline in oxygen concentration across the pycnocline to zero in the brine.

Beam attenuation data showed a slight peak in light attenuation in the surface mixed layer, then returned to near clear-water values in the midwater column to the depth of the pycnocline (**Figure 2**). Beam attenuation was at its greatest (8.6 m^{-1}) at a depth of 2,237.5 m, with two additional peaks near the top of the pycnocline (8.5 m^{-1} at 2,231.0 m; 8.4 m^{-1} at 2,236.5 m; **Figure 3**). Of the four CTD profiles taken by the ship's CTD (three) and the profiling camera (one) within the confines of northern Orca Basin, three showed similar peaks in beam attenuation near a depth of 2,238 m. Within the transition zone, thin layers of temperature variations were observed in addition to rapid changes of salinity, CDOM concentration, and total particle volume with depth (**Figure 4**).

Loss of image data, blackout, blurriness

Within the transition zone, characteristics of the marine snow particles changed rapidly, from numerous small ones, to very high concentrations of particulate matter causing complete loss of image data (blackout), to large

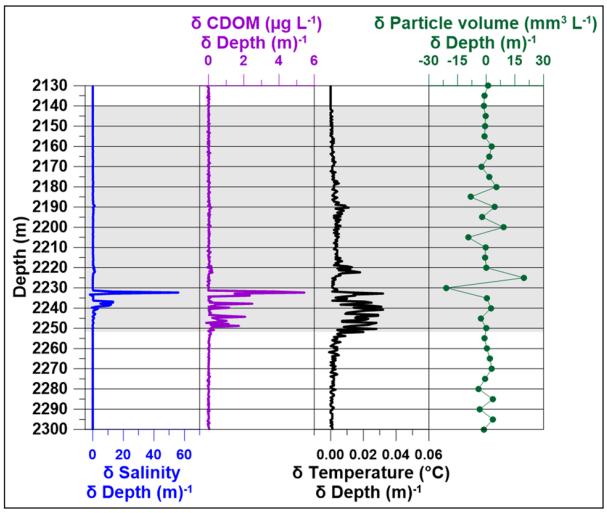

Figure 4: Changes in salinity, CDOM concentration, temperature, and total particle volume with depth. Changes in salinity, CDOM concentration, temperature, and total particle volume with depth are plotted, highlighting differences in the individual parameters across the interface from normal seawater to salt brine. Strongest changes in salinity were at 2,232 m and between depths of 2,236 m and 2,240 m. CDOM concentration changed in several steps between depths of 2,232 m and 2,250 m similarly to observed changes in temperature. Changes in total particle volume include a decrease at the first small change in salinity near 2,187 m followed by gains and losses at greater depths, with a notable increase near 2,225 m followed by a strong decrease suggesting loss of particulate mass. Shaded area indicates the transition zone. DOI: https://doi.org/10.1525/elementa.348.f4

aggregates below the depths of image blackouts. Both camera strobes were working, as can be detected in the image data; however, no individual particles were visible in the images and the images recorded were illuminated only very faintly near the edges where the strobes were located. The comet-shaped marine snow aggregates below these blacked-out images measured centimeters in length and a few millimeters in width (**Figures 3**, S4 and S5). Additional distinct layers of large numbers of small marine snow particles were observed in the transition zone. The 2.5-cm thick transition zone in the settling cylinder resembles natural conditions in Orca Basin with respect to salinity conditions and, on a different scale, the observed cloudy transition zone in the image data (Figures S4 and S5) between 2,140 m and 2,251 m.

Laboratory marine snow settling behavior

Marine snow aggregates tested in the laboratory ranged in size between 3 and 7 mm ESD (**Table 2**). All aggregates settled through the 2.5-cm thick transition zone between the overlying seawater and the brine in about 5 to 12 min; two of them broke up while settling through the pycnocline. Aggregate settling speeds (**Table 2**) ranged between 592 and 1,113 m d^{-1} in the overlying seawater, but slowed in the transition zone between seawater and brine to 3–9 m d^{-1} or 0.4–1.3% of their speed in seawater. Once in the brine, the aggregates settled at 181–402 m d^{-1} or 30.9–44.7% of their speed in seawater (**Table 2**).

Basin chemistry

CDOM concentrations in the upper water column were near the detection limit of ~0.02 µg L^{-1}, but rose abruptly below the pycnocline to 30.84 µg L^{-1} ± 6.75 µg L^{-1} (n = 15; **Figure 3**). CDOM concentrations correlated well with DOC concentrations (r^2 = 0.92, n = 15) obtained through laboratory analyses. CDOM concentrations were approximately 12% of the DOC concentration. Geochemistry determined from water samples collected during CTD Cast EN005.03 (**Table 3**) changed dramatically within the ~100-m halocline of northern Orca Basin. DOC concentrations increased six-fold, from 45–76 µM DOC in the seawater above 2,200 m to 278.3 µM DOC in the core of the brine at 2,250 m. CDOM concentrations paralleled DOC concentrations, increasing from 0.14 µg L^{-1} to 35.84 µg L^{-1} at depth (**Table 3**). Similarly, chloride and sodium concentrations increased sharply from 555.5 mM Cl^- and 453.1 mM Na^+ at a depth of 2,100 m to 4,967 M Cl^- and 4,667 mM Na^+ at 2,250 m. Conversely, potassium (K^+), manganese (Mg^{2+}), and calcium (Ca^{2+}) concentrations all decreased through the chemocline, ranging from seawater values of 9.0 mM K^+, 50.9 mM Mg^{2+}, and 9.9 mM Ca^{2+} above a depth of 2,200 m to 6.3 mM K^+, 11.3 mM Mg^{2+}, and 8.6 mM Ca^{2+} at 2,260 m (**Table 3**).

There were two interesting geochemical anomalies in these data, one near the top of the chemocline at 2,200 m and one at 2,300 m, the deepest sample at Orca North. While magnesium concentrations generally decreased from seawater to brine, both potassium and calcium reached local concentration maxima of 11.5 mM K^+ and 17.6 mM Ca^{2+} at 2,235 m (2.6 M Cl^- isopycnal surface). Potassium and calcium concentrations decreased thereafter to minima of 2.5 mM K^+ and 2.9 mM Ca^{2+} at 2,300 m depth. Despite apparent density differences, water column geochemical components shifted again at 2,300 m in the direction of seawater values, consistent with the early work of LaRock et al. (1979) who reported a possible shift in phosphate at 2,338 m. Chloride concentrations diminished from a maximum of 4.96 M at 2,260 m to 733 mM at 2,300 m, an approximate 7-fold dilution. DOC concentrations dropped from 277 µM at 2,260 m to 89 µM (a 3-fold dilution), and sodium concentrations from 4.67 M to 662 mM (a 7-fold dilution). Magnesium concentrations increased slightly, from 11.3 mM at 2,260 m to 13.6 mM at 2300 m, but the CDOM response remained nearly constant at 35.84 µg L^{-1}.

Transition zone from seawater to brine

Salinity increased slowly from 35 at 2,140 m to 61 at 2,229 m and then increased rapidly to >90 at 2,230 m (**Figures 2** and **3**) Below 2,230 m the salinity continued to increase to a maximum salinity of 318.1. Due to limits of the CTD to measure salinity above 90, laboratory geochemical data were used to estimate brine salinity, which was >300 (R Sibert, personal observation).

Table 2: Laboratory aggregate settling speeds, using roller-tank-generated marine snow aggregates and filtered Orca Basin brine and seawater from the deep Gulf of Mexico in graduated cylinder settling experiments. DOI: https://doi.org/10.1525/elementa.348.t2

Aggregate #	ESD (mm)	Settling speed (m d^{-1})			Percentage of settling speed of seawater (%)	
		Seawater	Transition	Brine	Transition	Brine
1	6	1,113	5	343	0.4	30.9
2	3	796	8	355	1.0	44.6
3	3	592	7	231	1.1	39.1
4[a]	5	912	3	258	0.3	28.3
5	3	613	4	224	0.6	36.6
6	2	549	3	181	0.5	32.9
7[a]	3	920	9	396	1.0	43.0
8	7	1,013	3	360	0.3	35.5
9	3	986	5	390	0.5	39.5
10	4	1,037	6	402	0.5	38.8
11	3	591	8	264	1.3	44.7

[a] Aggregate broke into two parts while settling through the pycnocline.

Table 3: R/V *Endeavor* CTD data and camera CDOM Station EN_005.03, Orca North, 27° 00.43' N, 91° 17.13' W, 15:15 UTZ. DOI: https://doi.org/10.1525/elementa.348.t3

Depth (m)	DOC (μM)	CDOM[a] (μg L^{-1})	Chloride (mM)	Na^+ (mM)	K^+ (mM)	Mg^{2+} (mM)	Ca^{2+} (mM)	Salinity[c]
2,100	76.0	0.14	555.5	453.1	9.0	50.9	9.9	35.6
2,175	45.0	1.01	639.5	535.5	10.2	51.0	10.6	41.0
2,200	51.7	2.65	850.7	740.1	8.3	38.6	8.8	54.5
2,235	182.5	19.98	2,645	2,412	11.5	30.2	17.6	169.4
2,245	244.0	28.53	4,754	4,328	5.7	11.2	9.0	304.5
2,250	278.3	34.49	4,967	4,668	6.2	11.2	8.6	318.1
2,260	276.8	35.37	4,961	4,566	6.3	11.3	8.6	317.7
2,300	89.2	35.84	733.3[b]	662.5	2.5	13.6	2.9	47.0

[a] Collected by the ECO_FLNTU sensor on the camera frame.
[b] A very low chloride concentration for this depth.
[c] Values above 90 calculated as salinity = 1.80655 * chloride.

Discussion

Based on the high resolution bathymetry by Kramer and Shedd (2017), an updated size of the Orca Basin was calculated. The previously suggested 1,800-m depth contour as the border for the Basin was deepened to 2,100 m, the depth of the outflow sill into Jefferson Basin in the NE quadrant of the Orca Basin, as the 1,800-m isobath extends beyond the actual confines of the Basin, downslope into other morphologically independent areas (**Figure 1**). This change in depth limit for the Basin reduces the 2-D surface area from ~400 km^2 (Shokes et al., 1977) to ~224 km^2. The permanent halocline (Sheu et al., 1990; Tribovillard et al., 2008) then covers an area of 158 km^2, having a volume of 10.24 km^3.

A major source of the particulate material present in the transition zone in the nepheloid layer above the brine arrives in the form of marine snow settling through the water column. This marine snow is supplied by surface production, lateral advection and resuspension from along an interface. As shown in previous studies in the Gulf of Mexico (Diercks and Asper, 1997; Ziervogel et al., 2016; Diercks et al., 2018), marine snow profiles display an increase in particle concentration near the seafloor over a water-column thickness of approximately 200 m (Diercks et al., 2018), indicative of a benthic nepheloid layer (BNL), a common occurrence in the world ocean (Gardner et al., 2017, 2018). The marine snow abundance in Orca Basin reported here exhibited similar characteristics to other Gulf of Mexico profiles, with a 200-m thick layer of elevated particle concentrations extending upwards from the top of the brine to a water depth of approximately 1,980 m (**Figure 2**). A unique aspect of the Orca Basin is that the

nepheloid layer, observed in the camera and transmissometer data, is not near the seafloor, but instead is situated atop the hypersaline brine. This nepheloid layer is likely generated by the strong density gradient of ~3 σ-units m^{-1} (Wiesenburg, 1980). For comparison, the gradients in the water columns of other anoxic regions, the Saanich Inlet, Cariaco Trench and Black Sea, are 0.01–0.3 σ-units m^{-1} (Richards, 1965).

Given the strong density gradient in the pycnocline, physical processes acting on particles in this zone may be similar to those in a typical BNL, particularly in terms of residence time. The particle residence time within the BNL is important for the recycling of the primary flux of biogenic material, as it extends the time that particles are exposed to remineralization (Walsh, 1992). Gardner et al. (1985) estimated residence times within the BNL from sediment trap data in the North Atlantic to be on the order of weeks to months. Residence times in the Fram Strait, estimated by van der Loeff et al. (2002), were on the order of 1–2 months. Calculations using laboratory measured settling speeds of 3–9 m d^{-1} (**Table 2**) in this study indicate that 11–34 days would be required for marine snow aggregates to settle undisturbed through 111 m of the transition zone in Orca Basin (2,140 and 2,251 m depths based on image data; Figures S4 and S5). This duration, though similar to the residence time of particles in BNLs, is likely an underestimation, as currents and turbulence were absent in the laboratory experiments, thus biasing settling speeds of the particles towards faster descent times.

The loss in particle volume associated with the top of the pycnocline, as indicated by the spike in salinity changes (**Figure 4**) and increase in CDOM and DOC concentrations (**Figures 3** and **4**), suggest that some of the particulate matter dissolved, contributing to the CDOM pool. Strong variations in particle concentration were associated with the changes in temperature and salinity around depths of 2,187 m and 2,225 m. In these specific cases, the camera crossed through thin bands, indicating loss of beam transmission possibly caused by layers of very high particle concentration (Figures S4 and S5). DOC concentrations were slightly lower but in good agreement with those published by Shah et al. (2013).

Both image sequences presented in Figures S4 and S5 illustrate the high variability of the particle abundance in size and numbers, as well as the high concentration of fine material that the camera cannot resolve but was recorded by the transmissometer. In several images of the sequences, the camera first recorded cloudiness, then blurry out-of-focus images followed by nearly completely blacked-out images. Below the blacked-out images, the water column was again clear, but with very large aggregates visible.

Layers of increased particulate Mn, an optically opaque particle, were reported by Trefry et al. (1984) below the water depth of 2,000 m with a maximum around 2,050 m, whereas Van Capellen et al. (1988) found the highest concentration of particulate Mn at 2,200 m in the South Orca Basin. Similar layers of high concentrations of particulate Mn were observed in the Black Sea at the interface between oxic and anoxic water masses (Honjo et al., 1988). The blacked-out images in our camera profile were reanalyzed and showed distinct changes in pixel values near their left and right edges where the strobe heads were located, indicating that both camera flashes were fired; however, their light was attenuated before it could be detected and recorded by the camera chip. In addition to these layered transitions of small aggregates, blurriness and elongated comet-shaped aggregates, several centimeters in length (similar to those shown in Figures S4 and S5), were recorded in a 27-m thick layer between 2,342 m and 2,369 m (images END_9137 to END_9153).

A large fraction of the particulate matter settling into the Basin is trapped within the high-density waters of the salinity transition (Millero et al., 1979), which results in a pronounced maximum of the particulate matter in the transition zone. Trefry et al. (1984) reported an increase in total suspended matter of up to 880 μg L^{-1} in the transition zone of Orca Basin, compared to 20–60 μg L^{-1} above 2,100 m and 200–400 μg L^{-1} below 2,250 m. However, they did not observe a peak in total suspended matter at the 2,190 m depth where Van Capellen et al. (1998) found their peak in manganese and our data show a distinct peak in particle concentration. This discrepancy could be due to differences in sampling location. Though Trefry et al. (1984) did not report specific sampling locations within Orca Basin, the locations of Van Capellen et al. (1998) were in South Orca Basin. Sager et al. (2003) suggested that the seawater-brine interface in the Orca Basin is enriched in particulate metal sulfides, which accumulate due to the strong density gradient at this interface. Metal sulfides are optically opaque, thus attenuating and scattering light more effectively than amorphous organic aggregates.

In Orca Basin, marine snow retained at the pycnocline consisted of up to 60% organic matter (Trefry et al., 1984; Van Cappellen et al., 1998). Wong et al. (1985) and Sheu (1983) reported that the settling organic matter was trapped at the pycnocline long enough to undergo a detectable degradation that was reflected by a strong release of biogenic iodine at the density interface, a component that responds strongly to the excitation wavelength of the ECO-FLNTU used during our camera deployment (**Figure 3**). Wong et al. (1985) suggested that the rapid decrease in the observed peak in total iodine concentration, from 8.1 μM in the transition zone at 2,266 m to 3.8 μM below 2,300 m, may have been caused by (1) an advective core of water with high dissolved iodine, (2) a horizontal diffusive flux of iodide from surrounding sediments on the slopes, or (3) an *in situ* preferential remineralization of biogenic particles that had accumulated along the pycnocline.

We suggest that lateral input of material explains the particle maximum captured in the camera-mounted CTD data near the depth of 2,230 m. Lateral flow would introduce material into the nepheloid layer atop the brine. Allen and Durrieu de Madron (2009) presented evidence that deep-sea canyons enhance cross-isobath flow, thus allowing upwelling and downwelling along the canyon axis. A canyon-like structure is identified in the NW corner of the morphology of the Orca Basin, due west of the camera deployment site (**Figure 1**). Based on data presented

by Allen and Durrieu de Madron (2009), we suggest that near inertial currents, as reported by Spencer et al. (2016), introduce ageostrophic flow conditions on the deep-sea floor across the canyon morphology, directing particle-laden, colder up-slope water into northern Orca Basin above the transition zone. This water mass then spreads, similarly to the Mississippi River plume at the sea surface, on top of the pycnocline, producing a spatially limited nepheloid layer similar in shape and size to that found as BNL in the northern Gulf of Mexico (Diercks et al., 2018) and in marine environments around the world (Gardner et al., 2018), or as intermediate nepheloid layers as suggested by Masunaga et al. (2017) for Otuschi Bay, Japan. No current meter data in Orca Basin are presently available to support this hypothesis directly, but we argue that the current meter data near the seafloor in water depths of 1,600 m in the northern Gulf of Mexico, indicating annual maximum current speeds of 18–20 cm s^{-1} (Spencer et al., 2016), are similar in scale and can produce small resuspension events as reported by Diercks et al. (2018).

A second mechanism we suggest, more pronounced in South Orca Basin due to the extent of the exposed salt dome, is the introduction of material via density-driven brine flow from the exposed salt dome in the SE corner of Orca Basin. The fresh brine originating on the slope of the slump surface in the SE corner can resuspend and transport material on the slopes from the salt dome, introducing this material into the transition zone.

The pycnocline constitutes a temporary barrier for marine snow, as presented in our laboratory settling experiments and in the marine snow abundance profile. In this transition zone, marine snow particles exchange pore water (Ploug et al., 2002; Prairie et al., 2013; Prairie and White, 2017) and settle at a reduced speed, which is proportional to the loss in excess density of the particles relative to the increased density of the brine solution. The results of our laboratory settling column experiments show that settling particles slow significantly upon entering the transition zone where salinity is rising steeply, similar to observations for midwater density stratifications presented by Prairie et al. (2013, 2015). Some of the material arriving from above will settle quickly through the pycnocline into the brine, while other material will be subject to fluid shear stress along this interface and become entrained in the nepheloid layer situated on top of the pycnocline, visible in our camera and transmissometer data. We suggest that marine snow particles in this transition zone above the salt brine experience similar changes as those in benthic nepheloid layers, which include aggregation, disaggregation, grazing, dissolution, microbial diffusion (Ploug et al., 2008) and finally sedimentation into the brine or, as under normal oceanographic settings, onto the seafloor.

The laboratory experimental results presented here also confirm that marine snow particles can traverse through the halocline present in Orca Basin. Our experimental transition zone of 2.5 cm thickness retained marine snow aggregates for several minutes, slowing them to 0.3–1.3% of their original speed before they continued to settle within the brine at 28–44% of their speed in the upper water column (**Table 3**). Prairie et al. (2013, 2015) reported two potential mechanisms as the main reasons for the delayed settling of aggregates through strong pycnoclines: 1) the entrainment of lower density pore fluids from above; and 2) changes in density of the particles due to their porosity. Both reasons depend on the permeability as well as the porosity of the particle which control the exchange of its pore water with the surrounding brine. Further, Jenkinson and Sun (2010) suggested that higher polymer viscosity, found at the top of pycnoclines and associated with high polymeric DOC content, slows the settling speed of particles. Faas (1991) and McAnally et al. (2007) suggested that a high concentration of particulate organic matter in the settling particles can have a similar effect on the settling speed of particles.

The delayed settling of marine snow aggregates in the transition zone can have significant consequences for local carbon cycling, as these aggregates often represent hot spots of bacterial activity (Smith et al., 1992; Kiørboe et al., 2002; Ziervogel et al., 2010; Prairie et al., 2015). The partial dissolution of organic matter within aggregates, and with it the formation of DOC, was attributed by Smith et al. (1992) to hydrolytic ectoenzymes exuded by the particle-associated bacteria. Leakage of the resulting organic solutes from sinking aggregates was suggested by Kiørboe and Jackson (2001) to contribute to water column bacterial production. Prairie et al. (2017) showed that bacteria and ectoenzymes originally associated with sinking marine snow detach from these aggregates at transition zones, remaining active in the layer long after the aggregates have settled out of these zones.

The average concentration of CDOM in the brine (30.84 $\mu g\ L^{-1} \pm 6.75\ \mu g\ L^{-1}$; n = 15), given the calculation of brine volume as described above, results in a total of 315.9 t of dissolved organic matter being stored in the brine. CDOM, at 12% of laboratory-measured DOC, paralleled the DOC concentration as it increased in the brine, suggesting that DOC is being released in the transition zone and stored within the brine. DOC concentration followed particle size and, inversely, volume distribution; i.e., a loss in total particle volume and an increase in total particle numbers were observed at the depths where DOC concentration increased.

The mean of measured DOC concentrations in the brine, 241.0 $\mu M \pm 65.2\ \mu M$ (n = 10), results in a total amount of 2.47×10^9 moles of DOC stored in the brine, providing a potential source of (refractory) DOC for the abiotic formation of marine snow aggregates as described by (Hansell et al., 2009); in fact, comet-shaped marine snow aggregates several centimeters in length, not seen higher in the water column, were observed just below the transition zone. Some of the DOC comes in with the salt (Joye et al., 2010), but Shah et al. (2013) have also suggested microbial conversion (enzymatic hydrolysis) of POC to DOC, as well as physical disaggregation of POC into DOC, based on stable C isotope budgets evaluated across the chemocline.

Summary

The data presented in this paper present the first continuous profile of marine snow distribution in the Orca Basin. Recorded concentrations of marine snow highlight the physical settings of the permanent halocline, with the pres-

ence of a nepheloid layer of small particle sizes above this interface and large aggregates below in the brine, containing a higher volume of aggregated material due to reduced settling speeds in the brine, as shown in the presented laboratory data on settling speed. We suggest that physical, chemical, and biological alteration of material arriving from the surface and through lateral advection into the lower water column and the transition zone lead to increased CDOM and DOC concentrations in the transition zone and in the brine. The transition zone between normal seawater and the brine is a very dynamic part of the water column, characterized by processes similar to those in the transition of water to sediment at the seafloor, but with vertical export into brine instead of sediment.

Data Accessibility Statement

Data are publicly available through the Gulf of Mexico Research Initiative Information & Data Cooperative (GRIIDC) at https://data.gulfresearchinitiative.org.

- Camera data: https://doi.org/10.7266/N7251G72
- Geochemical data: https://doi.org/10.7266/n7-3bp5-sb94
- Hydrographic data: https://doi.org/10.7266/N7R-R1WKK

Supplemental files

The supplemental files for this article can be found as follows:

- **Figure S1.** A 3D rendering of the seafloor morphology of the Orca Basin. DOI: https://doi.org/10.1525/elementa.348.s1
- **Figure S2.** Beam attenuation profiles through the transition zone. DOI: https://doi.org/10.1525/elementa.348.s1
- **Figure S3.** Temperature–salinity diagram for North Orca Basin camera station. DOI: https://doi.org/10.1525/elementa.348.s1
- **Figure S4.** Sequence of images from the profiling camera entering the transition zone. DOI: https://doi.org/10.1525/elementa.348.s1
- **Figure S5.** Sequence of images from the profiling camera deeper into the transition zone. DOI: https://doi.org/10.1525/elementa.348.s1
- **Figure S6.** Enlargement of the transition zone created in the graduated cylinder. DOI: https://doi.org/10.1525/elementa.348.s1

Acknowledgements

We thank the science party and ship's crew of the *RV Endeavor*.

Funding information

This research was made possible by a grant from The Gulf of Mexico Research Initiative to support the ECOGIG-2 research consortium. This is ECOGIG contribution 518.

Competing interests

The authors have no competing interests to declare.

Author contributions

- Contributed to conception and design: ARD, KZ, RS, SJ, JM
- Contributed to acquisition of data: ARD, KZ, RS, SJ, JM
- Contributed to analysis and interpretation of data: ARD, KZ, RS, SJ, JM
- Drafted and/or revised the article: ARD, VLA, KZ, RS, SJ
- Approved the submitted version for publication: ARD, VLA, KZ, RS, SJ, JM

References

Addy, SK and **Behrens, EW.** 1980. Time of accumulation of hypersaline anoxic brine in Orca basin (Gulf of Mexico). *Mar Geol* **37**(3): 241–252. DOI: https://doi.org/10.1016/0025-3227(80)90104-8

Allen, SE and **de Madron, XD.** 2009. A review of the role of submarine canyons in deep-ocean exchange with the shelf. *Ocean Sci* **5**(4): 607–620. DOI: https://doi.org/10.5194/os-5-607-2009

Asper, VL. 1987. Measuring the flux and sinking speed of marine snow aggregates. *Deep Sea Res* **34**(1): 1–17. DOI: https://doi.org/10.1016/0198-0149(87)90117-8

Condie, SA and **Bormans, M.** 1997. The Influence of Density Stratification on Particle Settling, Dispersion and Population Growth. *J Theor Biol* **187**(1): 65–75. DOI: https://doi.org/10.1006/jtbi.1997.0417

Diercks, A-R and **Asper, VL.** 1997. In situ settling speeds of marine snow aggregates below the mixed layer: Black Sea and Gulf of Mexico. *Deep Sea Res* **44**(3): 385–398. DOI: https://doi.org/10.1016/S0967-0637(96)00104-5

Diercks, A-R, Dike, C, Asper, VL, DiMarco, SF, Chanton, JP and **Passow, U.** 2018. Scales of seafloor sediment resuspension in the northern Gulf of Mexico. *Elem Sci Anth* **6**(1): 32. DOI: https://doi.org/10.1525/elementa.285

Ducklow, H, Steinberg, D and **Buesseler, K.** 2001. Upper ocean carbon export and the biological pump. *Oceanography* **14**(4): 50–58. DOI: https://doi.org/10.5670/oceanog.2001.06

Faas, RW. 1991. Rheological boundaries of mud: Where are the limits? *Geo-Mar Lett* **11**(3): 143–146. DOI: https://doi.org/10.1007/BF02431000

Gardner, WD, Richardson, MJ and **Mishonov, AV.** 2018. Global assessment of benthic nepheloid layers and linkage with upper ocean dynamics. *Earth Planet Sci Lett* **482**: 126–134. DOI: https://doi.org/10.1016/j.epsl.2017.11.008

Gardner, WD, Southard, JB and **Hollister, CD.** 1985. Sedimentation, resuspension and chemistry of particles in the northwest Atlantic. *Mar Geol* **65**(3): 199–242. DOI: https://doi.org/10.1016/0025-3227(85)90057-X

Gardner, WD, Tucholke, BE, Richardson, MJ and **Biscaye, PE.** 2017. Benthic storms, nepheloid layers, and linkage with upper ocean dynamics in the western North Atlantic. *Mar Geol* **385**: 304–327. DOI: https://doi.org/10.1016/j.margeo.2016.12.012

Hansell, D, Carlson, C, Repeta, D and **Schlitzer, R.** 2009. Dissolved organic matter in the ocean: A controversy stimulates new insights. *Oceanography* **22**(4): 202–211. DOI: https://doi.org/10.5670/oceanog.2009.109

Honjo, S, Doherty, KW, Agrawal, YC and **Asper, VL.** 1984. Direct optical assessment of large amorphous aggregates (marine snow) in the deep ocean. *Deep Sea Res* **31**: 67–76. DOI: https://doi.org/10.1016/0198-0149(84)90073-6

Honjo, S, Hay, BJ and **Party M of the SS.** 1988. Temporal and spatial variability in sedimentation in the Black Sea: Cruise report R/V Knorr 134–8, Black Sea Leg 1, April 16–May 7, 1988. Woods Hole Oceanographic Institution. DOI: https://doi.org/10.1575/1912/1230

Hurtgen, MT, Lyons, TW, Ingall, ED and **Cruse, AM.** 1999. Anomalous enrichments of iron monosulfide in euxinic marine sediments and the role of H_2S in iron sulfide transformations; examples from Effingham Inlet, Orca Basin, and the Black Sea. *Am J Sci* **299**(7–9): 556–588. DOI: https://doi.org/10.2475/ajs.299.7-9.556

Jenkinson, IR and **Sun, J.** 2010. Rheological properties of natural waters with regard to plankton thin layers. A short review. *J Mar Syst* **83**(3): 287–297. DOI: https://doi.org/10.1016/j.jmarsys.2010.04.004

Joint Panel on Oceanographic Tables. 1966. *Second Report of the Joint Panel on Oceanographic Tables and Standards: Rome, 8–9 October 1965*. UNESCO. (UNESCO technical papers in marine science).

Joye, SB, Bowles, MW, Samarkin, VA, Hunter, KS and **Niemann, H.** 2010. Biogeochemical signatures and microbial activity of different cold-seep habitats along the Gulf of Mexico deep slope. *Deep Sea Res Part II* **57**(21–23): 1990–2001. DOI: https://doi.org/10.1016/j.dsr2.2010.06.001

Kaminskii, ST, Kotovshchikov, BB and **Markov, AA.** 1989. Peculiarities of the formation of the cold intermediate layer in Black Sea regions with various dynamic conditions. *Sov J Phys Oceanogr* **1**(2): 121–128. DOI: https://doi.org/10.1007/BF02198022

Kindler, K, Khalili, A and **Stocker, R.** 2010. Diffusion-limited retention of porous particles at density interfaces. *Proc Natl Acad Sci* **107**(51): 22163–22168. DOI: https://doi.org/10.1073/pnas.1012319108

Kiørboe, T, Grossart, H-P, Ploug, H and **Tang, K.** 2002. Mechanisms and rates of bacterial colonization of sinking aggregates. *Appl Environ Microbiol* **68**(8): 3996–4006. DOI: https://doi.org/10.1128/AEM.68.8.3996-4006.2002

Kiørboe, T and **Jackson, GA.** 2001. Marine snow, organic solute plumes, and optimal chemosensory behavior of bacteria. *Limnol Oceanogr* **46**(6): 1309–1318. DOI: https://doi.org/10.4319/lo.2001.46.6.1309

Kramer, KV and **Shedd, B.** 2017. A 1.4-Billion-Pixel Map of the Gulf of Mexico Seafloor. *Eos*. Available at: https://eos.org/project-updates/a-1-4-billion-pixel-map-of-the-gulf-of-mexico-seafloor. Accessed 2018 Jan 11.

LaRock, PA, Lauer, RD, Schwarz, JR, Watanabe, KK and **Wiesenburg, DA.** 1979. Microbial biomass and activity distribution in an anoxic, hypersaline basin. *Appl Env Microbiol* **37**: 466–470.

Leventer, A, Williams, DF and **Kennett, JP.** 1983. Relationships between anoxia, glacial meltwater and microfossil preservation in the Orca Basin, Gulf of Mexico. *Mar Geol* **53**(1): 23–40. DOI: https://doi.org/10.1016/0025-3227(83)90032-4

Masunaga, E, Arthur, RS, Fringer, OB and **Yamazaki, H.** 2017. Sediment resuspension and the generation of intermediate nepheloid layers by shoaling internal bores. *J Mar Syst* **170**: 31–41. DOI: https://doi.org/10.1016/j.jmarsys.2017.01.017

McAnally, WH, Friedrichs, C, Hamilton, D, Hayter, E, Shrestha, P, Rodriguez, H, Sheremet, A and **Teeter, A.** 2007. Management of fluid mud in estuaries, bays, and lakes. I: Present state of understanding on character and behavior. *J Hydraul Eng* **133**(1): 9–22. DOI: https://doi.org/10.1061/(ASCE)0733-9429(2007)133:1(9)

McKee, TR, Jeffrey, LM, Presley, BJ and **Ii, UGW.** 1978. Holocene sediment geochemistry of continental slope and intraslope basin areas, Northwest Gulf of Mexico: 5. Intraslope basins. In: *Framework, Facies, and Oil-Trapping Characteristics of the Upper Continental Margin* **117**: 313–326.

Meckler, AN, Schubert, CJ, Hochuli, PA, Plessen, B, Birgel, D, Flower, BP, Hinrichs, K-U and **Haug, GH.** 2008. Glacial to Holocene terrigenous organic matter input to sediments from Orca Basin, Gulf of Mexico — A combined optical and biomarker approach. *Earth Planet Sci Lett* **272**(1): 251–263. DOI: https://doi.org/10.1016/j.epsl.2008.04.046

Millero, FJ, Lo Surdo, A, Chetirkin, P and **Guinasso, NL.** 1979. The density and speed of sound of Orca Basin waters. *Limnol Oceanogr* **24**(2): 218–225. DOI: https://doi.org/10.4319/lo.1979.24.2.0218

Murray, GE. 1966. Salt structures of Gulf of Mexico Basin; a review. *Bull Am Assoc Pet Geol* **50**(3): 439–478. DOI: https://doi.org/10.1306/5D25B49D-16C1-11D7-8645000102C1865D

Pilcher, RS and **Blumstein, RD.** 2007. Brine volume and salt dissolution rates in Orca Basin, northeast Gulf of Mexico. *AAPG Bull* **91**(6): 823–833. DOI: https://doi.org/10.1306/12180606049

Ploug, H, Hietanen, S and **Kuparinen, J.** 2002. Diffusion and advection within and around sinking, porous diatom aggregates. *Limnol Oceanogr* **47**(4): 1129–1136. DOI: https://doi.org/10.4319/lo.2002.47.4.1129

Ploug, H, Iversen, MH and **Fischer, G.** 2008. Ballast, sinking velocity, and apparent diffusivity within marine snow and zooplankton fecal pellets: Implications for substrate turnover by attached bacteria. *Limnol Oceanogr* **53**(5): 1878–1886. DOI: https://doi.org/10.4319/lo.2008.53.5.1878

Prairie, JC and **White, BL.** 2017. A model for thin layer formation by delayed particle settling at sharp density gradients. *Cont Shelf Res*

133(Supplement C): 37–46. DOI: https://doi.org/10.1016/j.csr.2016.12.007

Prairie, JC, Ziervogel, K, Arnosti, C, Camassa, R, Falcon, C, Khatri, S, McLaughlin, R, White, B and **Yu, S.** 2013. Delayed settling of marine snow at sharp density transitions driven by fluid entrainment and diffusion-limited retention. *Mar Ecol Prog Ser* **487**: 185–200. DOI: https://doi.org/10.3354/meps10387

Prairie, JC, Ziervogel, K, Camassa, R, McLaughlin, RM, White, BL, Dewald, C and **Arnosti, C.** 2015. Delayed settling of marine snow: Effects of density gradient and particle properties and implications for carbon cycling. *Mar Chem* **175**: 28–38. DOI: https://doi.org/10.1016/j.marchem.2015.04.006

Prairie, JC, Ziervogel, K, Camassa, R, McLaughlin, RM, White, BL, Johnson, ZI and **Arnosti, C.** 2017 Nov 3. Ephemeral aggregate layers in the water column leave lasting footprints in the carbon cycle: Aggregate layers leave carbon footprints. *Limnol Oceanogr Lett* **2**: 202–209. DOI: https://doi.org/10.1002/lol2.10053

Sager, WW, MacDonald, IR and **Hou, R.** 2003. Geophysical signatures of mud mounds at hydrocarbon seeps on the Louisiana continental slope, northern Gulf of Mexico. *Mar Geol* **198**(1–2): 97–132. DOI: https://doi.org/10.1016/S0025-3227(03)00097-5

Schardt, C. 2016. Hydrothermal fluid migration and brine pool formation in the Red Sea: The Atlantis II Deep. *Miner Deposita* **51**(1): 89–111. DOI: https://doi.org/10.1007/s00126-015-0583-2

Shah, SR, Joye, SB, Brandes, JA and **McNichol, AP.** 2013. Carbon isotopic evidence for microbial control of carbon supply to Orca Basin at the seawater–brine interface. *Biogeosciences* **10**(5): 3175–3183. DOI: https://doi.org/10.5194/bg-10-3175-2013

Sheu, D-D. 1983. The Geochemistry of Orca Basin Sediments [Ph.D.]. [United States — Texas]: Texas A&M University. Available at: https://search-proquest-com.lynx.lib.usm.edu/docview/303303433/abstract/1AAD8B99E2640E2PQ/2.

Sheu, D-D. 1990. The anoxic Orca Basin (Gulf of Mexico): Geochemistry of brines and sediments. *Rev Aquat Sci* **2**: 491–507.

Sheu, D-D and **Presley, BJ.** 1986a. Formation of hematite in the euxinic Orca Basin, northern Gulf of Mexico. *Mar Geol* **69**(3–4): 309–321. DOI: https://doi.org/10.1016/0025-3227(86)90045-9

Sheu, D-D and **Presley, BJ.** 1986b. Variations of calcium carbonate, organic carbon and iron sulfides in anoxic sediment from the Orca Basin, Gulf of Mexico. *Mar Geol* **70**(1): 103–118. DOI: https://doi.org/10.1016/0025-3227(86)90091-5

Sheu, D-D, Shakur, A, Pigott, JD, Wiesenburg, DA, Brooks, JM and **Krouse, HR.** 1988. Sulfur and oxygen isotopic compositions of dissolved sulfate in the Orca Basin: Implications for origin of the high-salinity brine and oxidation of sulfides at the brine-seawater interface. *Mar Geol* **78**(3): 303–310. DOI: https://doi.org/10.1016/0025-3227(88)90115-6

Shokes, RF, Trabant, PK, Presley, BJ and **Reid, DF.** 1977. Anoxic, hypersaline basin in the northern Gulf of Mexico. *Science* **196**(4297): 1443–1446. DOI: https://doi.org/10.1126/science.196.4297.1443

Smith, DC, Simon, M, Alldredge, AL and **Azam, F.** 1992. Intense hydrolytic enzyme activity on marine aggregates and implications for rapid particle dissolution. *Nature* **359**(6391): 139–142. DOI: https://doi.org/10.1038/359139a0

Spencer, LJ, DiMarco, SF, Wang, Z, Kuehl, JJ and **Brooks, DA.** 2016. Asymmetric oceanic response to a hurricane: Deep water observations during Hurricane Isaac. *J Geophys Res Oceans* **121**(10): 7619–7649. DOI: https://doi.org/10.1002/2015JC011560

Trefry, JH, Presley, BJ, Keeney-Kennicutt, WL and **Trocine, RP.** 1984. Distribution and chemistry of manganese, iron, and suspended particulates in Orca Basin. *Geo-Mar Lett* **4**(2): 125–130. DOI: https://doi.org/10.1007/BF02277083

Tribovillard, N, Bout-Roumazeilles, V, Algeo, T, Lyons, TW, Sionneau, T, Montero-Serrano, JC, Riboulleau, A and **Baudin, F.** 2008. Paleodepositional conditions in the Orca Basin as inferred from organic matter and trace metal contents. *Mar Geol* **254**(1): 62–72. DOI: https://doi.org/10.1016/j.margeo.2008.04.016

Tribovillard, N, Bout-Roumazeilles, V, Sionneau, T, Serrano, JCM, Riboulleau, A and **Baudin, F.** 2009. Does a strong pycnocline impact organic-matter preservation and accumulation in an anoxic setting? The case of the Orca Basin, Gulf of Mexico. *Comptes Rendus Geosci* **341**(1): 1–9. DOI: https://doi.org/10.1016/j.crte.2008.10.002

Van Cappellen, P, Viollier, E, Roychoudhury, A, Clark, L, Ingall, E, Lowe, K and **Dichristina, T.** 1998. Biogeochemical cycles of manganese and iron at the oxic- anoxic transition of a stratified marine basin (Orca Basin, Gulf of Mexico). *Environ Sci Technol* **32**(19): 2931–2939. DOI: https://doi.org/10.1021/es980307m

van der Loeff, MR, Meyer, R, Rudels, B and **Rachor, E.** 2002. Resuspension and particle transport in the benthic nepheloid layer in and near Fram Strait in relation to faunal abundances and ^{234}Th depletion. *Deep Sea Res* **49**(11): 1941–1958. DOI: https://doi.org/10.1016/S0967-0637(02)00113-9

Walsh, I. 1992. Large aggregate flux and fate at the seafloor: Diagenesis during the rebound process. In: Rowe, GT and Pariente, V (eds.), *Deep-Sea Food Chains and the Global Carbon Cycle. NATO ASI Series (Series C: Mathematical and Physical Sciences)* **360**. Dordrecht: Springer. Available at: http://search.proquest.com/docview/16774062/?pq-origsite=primo. DOI: https://doi.org/10.1007/978-94-011-2452-2_22

Wei, C-L and **Murray, JW.** 1994. The behavior of scavenged isotopes in marine anoxic environments:

^{210}Pb and ^{210}Po in the water column of the Black Sea. *Geochim Cosmochim Acta* **58**(7): 1795–1811. DOI: https://doi.org/10.1016/0016-7037(94)90537-1

Wiesenburg, DA. 1980. Geochemistry of Dissolved Gases in the Hypersaline Orca Basin [Ph.D.]. [United States — Texas]: Texas A&M University. Available at: https://search-proquest-com.lynx.lib.usm.edu/docview/303001069/abstract/1AAD8B99E2640E2PQ/1.

Wiesenburg, DA, Brooks, JM and **Bernard, BB.** 1985. Biogenic hydrocarbon gases and sulfate reduction in the Orca Basin brine. *Geochim Cosmochim Acta* **49**(10): 2069–2080. DOI: https://doi.org/10.1016/0016-7037(85)90064-X

Wong, GTF, Takayanagi, K and **Todd, JF.** 1985. Dissolved iodine in waters overlying and in the Orca Basin, Gulf of Mexico. *Mar Chem* **17**(2): 177–183. DOI: https://doi.org/10.1016/0304-4203(85)90072-6

Ziervogel, K, Dike, C, Asper, V, Montoya, J, Battles, J, D'souza, N, Passow, U, Diercks, A, Esch, M, Joye, S, et al. 2016. Enhanced particle fluxes and heterotrophic bacterial activities in Gulf of Mexico bottom waters following storm-induced sediment resuspension. *Deep Sea Res Part II* **129**(Supplement C): 77–88. DOI: https://doi.org/10.1016/j.dsr2.2015.06.017

Ziervogel, K, Steen, AD and **Arnosti, C.** 2010. Changes in the spectrum and rates of extracellular enzyme activities in seawater following aggregate formation. *Biogeosciences* **7**(3): 1007–1015. DOI: https://doi.org/10.5194/bg-7-1007-2010

How to cite this article: Diercks, A, Ziervogel, K, Sibert, R, Joye, SB, Asper, V and Montoya, JP. 2019. Vertical marine snow distribution in the stratified, hypersaline, and anoxic Orca Basin (Gulf of Mexico). *Elem Sci Anth,* 7: 10. DOI: https://doi.org/10.1525/elementa.348

Domain Editor-in-Chief: Jody W. Deming, Department of Biological Oceanography, University of Washington, US

Associate Editor: Laurenz Thomsen, Department of Earth and Space Sciences, Jacobs University Bremen, DE

Knowledge Domain: Ocean Science

Part of an *Elementa* Special Feature: Impacts of Natural Versus Anthropogenic Oil Inputs on the Gulf of Mexico Ecosystem

Submitted: 10 August 2018 **Accepted:** 24 January 2019 **Published:** 14 February 2019

ELEMENTA Science of the Anthropocene

Elem Sci Anth is a peer-reviewed open access journal published by University of California Press.

OPEN ACCESS